Journal of Polymer Research (2020) 27: 26
https://doi.org/10.1007/s10965-019-1993-0

ORIGINAL PAPER

Effect of copper (II) nitrate $3H_2O$ on the crystalline, optical and electrical properties of poly(vinyl alcohol) films

R. S. Hafez[1] · S. El-Khiyami[1]

Received: 22 October 2019 / Accepted: 20 December 2019 / Published online: 3 January 2020

Abstract
Composite films of poly (vinyl alcohol) PVA doped with various weight ratios of $Cu(NO_3)_2.3H_2O$ (0, 1, 5, 10 and 20) wt% have been prepared by solution casting method. Using X-ray diffraction (XRD), Fourier transform infrared spectroscopy (FT-IR), and Ultraviolet–Visible (Uv-Vis) spectroscopy, the synthetic composites were analyzed. The findings showed that $Cu(NO_3)_2.3H_2O$ interacts with the hydroxyl group present in PVA chain. The XRD analysis revealed that after adding $Cu(NO_3)_2.3H_2O$, PVA crystallites were destroyed. With increasing $Cu(NO_3)_2.3H_2O$ ratio, the absorbance of composite samples increased. The optical band gap energy of the composite samples was calculated using Tauc's formula and it reduced by increasing dopant concentration. The dielectric modulus and ac conductivity of the composite films have been studied. Ac conductivity was found to increase by increasing the dopant concentration up to 10 wt%. Electrical conduction is carried out using correlated barrier hopping model.

Keywords PVA · Cu $(NO_3)_2.3H_2O$ · Optical properties · Electrical properties · FT-IR.1 introduction

Introduction

Polymeric materials are numerous and have excellent potential in many applications due to their versatility, low density, complex forms and low production cost. They can be found in medical equipment, automotive components, optical products, electronic circuits, space and military technology. Due to the type and the concentration of the filler used, the electrical and optical properties of the chosen polymer can be controllably changed [1].

PVA is one of the most important synthetic polymers with a broad variety of applications. The chemical and physical characteristics of PVA come from its hydroxyl group. In general, various additives are used to alter and enhance PVA characteristics and provide a high degree of durability against the environment. Inorganic additives have significant impact on the optical and electrical properties of PVA polymer. Optical, structural and other characteristics of PVA with various dopants such as NaCl, CuCl, ZnSe, CdS, NiCl2, MnCl, $MgBr_2$, CrF_3, $MgCl_2$, $Ca(NO_3)_2$, $Mg(NO_3)_2$ and $AgNO_3$ have been investigated by various research groups using different methods [2–15].

Copper Nitrate $Cu(NO_3)_2.3H_2O$ was doped into PVA to enrich the studies of the effect of various inorganic metal salts on the characteristics of PVA. This research studies the effect of $Cu(NO_3)_2.3H_2O$ on the structural, optical and electrical properties of PVA.

Experimental part

Materials

Polyvinyl alcohol [PVA. Alpha chemika, India] and Copper (II) nitrate $.3H_2O$ $Cu(NO_3)_2.3H_2O$ 99%. $M_w = 241.60$. SDFCL, India] were used as received without further purification. Distilled water was used as solvent throughout the experiment.

Preparation of PVA/$Cu(NO_3)_2.3H_2O$ composite films

Different compositions of PVA/ $Cu(NO_3)_2.3H_2O$ films have been prepared by solution casting method, using various weight ratios of $Cu(NO_3)_2$ $.3H_2O$ (0, 1, 5, 10 and 20) wt%. PVA and $Cu(NO_3)_2$ $.3H_2O$ solution is obtained by dissolving them in 100 ml of distilled water, and the solution is

✉ R. S. Hafez
rsaber@sci.cu.edu.eg

[1] Physics Department, Faculty of Science, Cairo University, Cairo 12613, Egypt

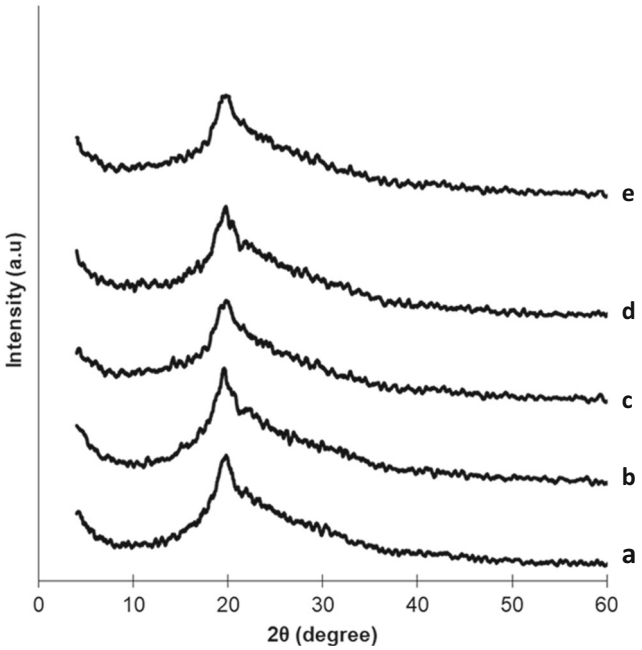

Fig. 1 X-ray diffraction patterns of: **a** 100/0, **b** 99/1, **c** 95/5, **d** 90/10 and **e** 80/20 (wt/wt%) PVA/ $Cu(NO_3)_2.3H_2O$ composite films

magnetically stirred continuously at room temperature for 3 h, until highly homogenous solution has been formed.

The final PVA/$Cu(NO_3)_2.3H_2O$ mixture was casted in glass dish, allowing the solvent to evaporate slowly for one week at room temperature. The obtained films were placed in a dust free chamber in order to prevent the moisture effect. The prepared films were uniform with an average thickness of 40 μm.

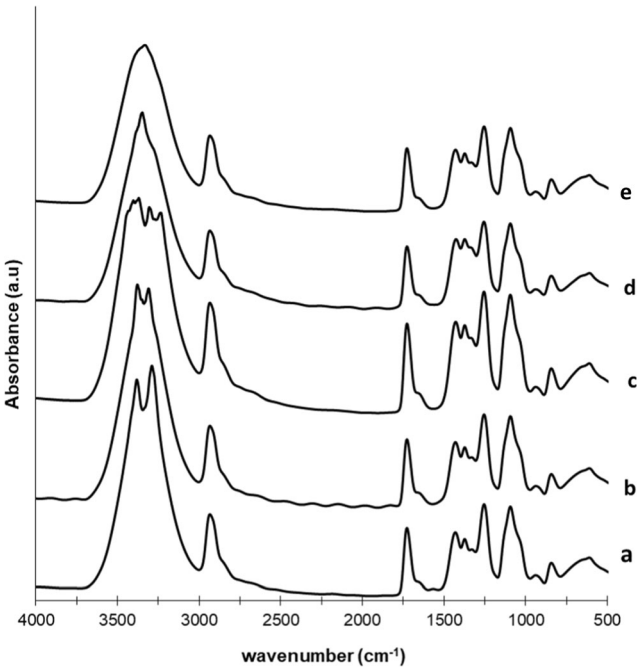

Fig. 2 FT-IR absorption spectra of: **a** 100/0, **b** 99/1, **c** 95/5, **d** 90/10 and **e** 80/20 (wt/wt%) PVA/ $Cu(NO_3)_2.3H_2O$ composite films

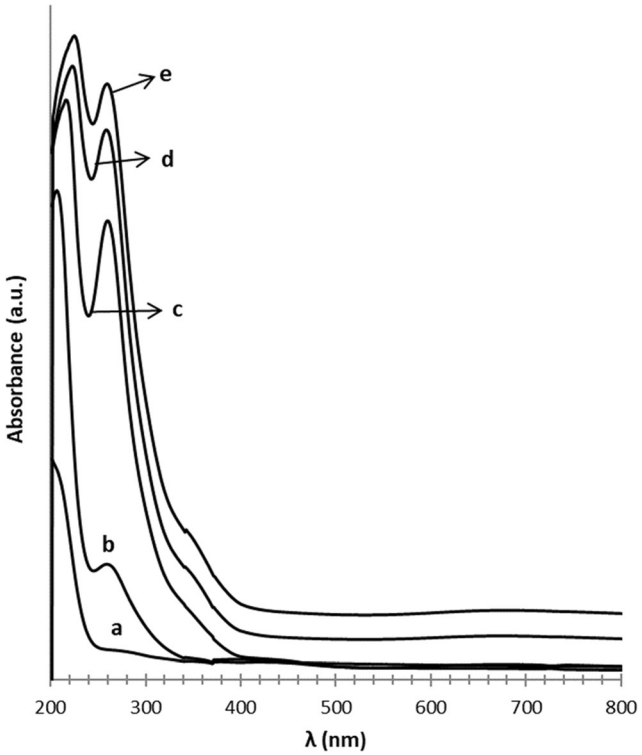

Fig. 3 UV-Vis absorption spectra of: **a** 100/0, **b** 99/1, **c** 95/5, **d** 90/10 and **e** 80/20 (wt/wt%) PVA/ $Cu(NO_3)_2.3H_2O$ composite films

Measurements

The pattern of X-ray diffraction (XRD) were obtained using X'PERT-PRO-PANalytical channel control using Cu-Kα target (λ = 1.5406 Å, scans were collected over a 2θ range of 5°-60°). FT-IR measurements were carried out in the spectral range of 4000–400 cm^{-1}using JASCO, FT/IR-6100. UV-Vis absorption spectra have been recorded in the wave length range of 200–800 nm using UV-630 (Shimadzu) UV-VIS-NIR spectrophotometer. Dielectric measurements were performed using Broadband Dielectric Spectroscopy (BDS) type Novocontrol concept 40.

Results and discussion

X-ray diffraction

XRD patterns of PVA and PVA/ $Cu(NO_3)_2.3H_2O$ composite films are shown in Fig. 1. Pure PVA spectrum shows a broad peak at approximately 2θ = 19.3° corresponding to (101)

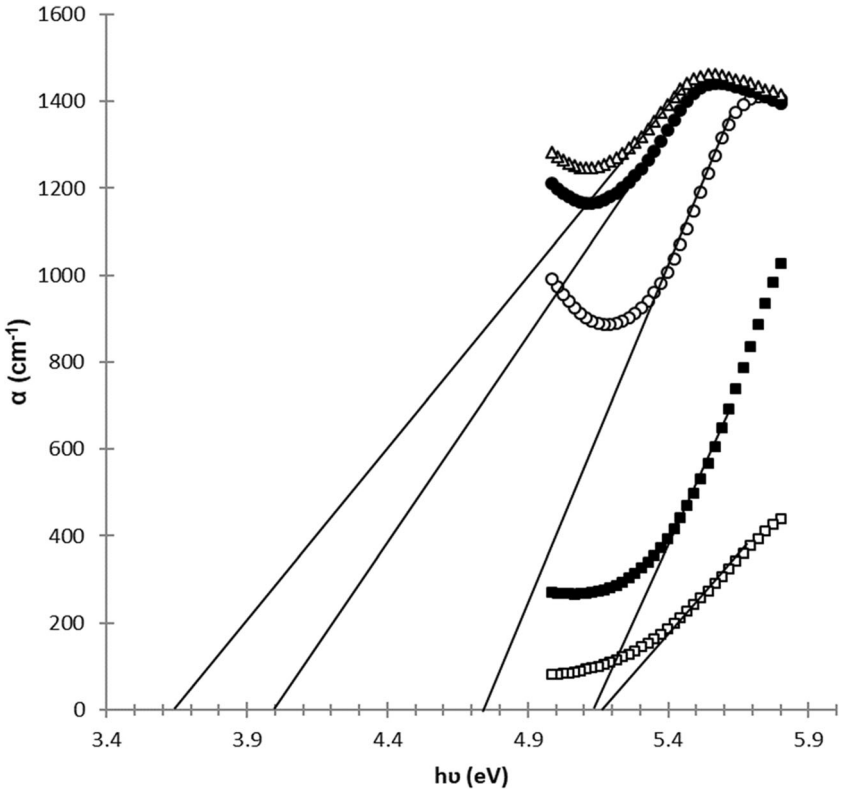

Fig. 4 Relation between absorption coefficient α (cm^{-1}) versus hυ (eV) for (□) 100/0, (■) 99/1, (○) 95/5, (●) 90/10 and (Δ) 80/20 (wt/wt%) PVA/ $Cu(NO_3)_2.3H_2O$ composite films

crystal plane [16, 17], indicating the semi-crystalline nature of PVA. The crystalline nature of PVA may be due to the strong interaction of hydrogen bond in the polymer chain between the hydroxyl groups [18]. For doped samples, the characteristic diffraction peak of PVA beings to decrease in intensity and increase in broadening. These results mean that adding $Cu(NO_3)_2.3H_2O$ reduces the crystallinity of PVA. Also, The absence of any new diffraction peaks for composite films implies a complete dissociation of $Cu(NO_3)_2.3H_2O$ on the polymer matrix.

Fourier transform infrared (FT-IR) spectroscopy

FT-IR spectroscopy is highly sensitive to hydrogen bond formation [19] and can be used to detect interactions in polymer composites. Figure 2 displays the FT-IR absorption spectra of pure PVA and PVA/ $Cu(NO_3)_2.3H_2O$ composite films. In the case of pure PVA (spectrum a), it appears that there is no appreciable difference in the absorption bands compared to the previously reported [17, 20]. The two absorption bands for PVA at 3369 cm^{-1} and 3276 cm^{-1} were attributed to O-H stretching vibration of hydroxyl group. The absorption band corresponding to C-H asymmetric stretching vibration occurred at 2914 cm^{-1}. The band at 1717 cm^{-1} is due to C=O stretching vibration of the remaining vinyl acetate group from PVA. The absorption band at 1415 cm^{-1} is caused by C-H symmetric bending of CH_2 in PVA back bone. A band at 1336 cm^{-1} is assigned to CH_2 wagging. The C-O-C stretching of the acetyl group on the back bone of PVA is ascribed to a band at 1080 cm^{-1}. For composite samples (spectra b-e), all spectra

Table 1 The values of the absorption edge, direct ($E_{g(direct)}$) band gap, indirect ($E_{g(indirect)}$) band gap and Urbach energy (E_U) of PVA/ $Cu(NO_3)_2.3H_2O$ composite films

Film composition PVA/$Cu(NO_3)_2.3H_2O$ (wt/wt%)	Absorption Edge (eV)	$E_{g(direct)}$ (eV)	$E_{g(indirect)}$ (eV)	E_U (eV)
100/0	5.18	5.30	4.70	0.41
99/1	5.15	5.15	4.60	0.74
95/5	4.75	5.05	4.05	1.58
90/10	4.00	4.80	3.00	2.09
80/20	3.65	4.70	2.60	2.49

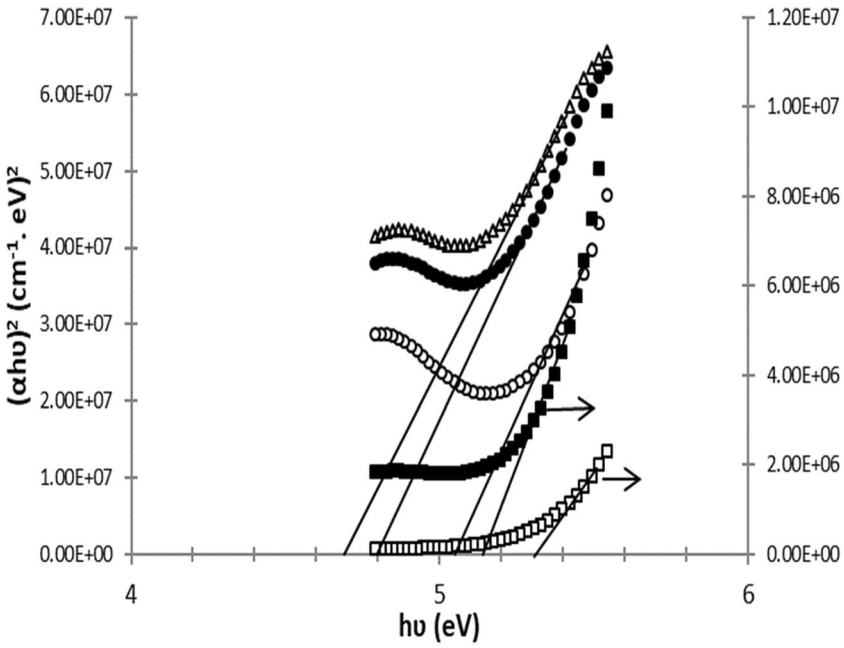

Fig. 5 Relation between $(\alpha h)^2$ $(cm^{-1}. eV)^2$ versus hυ (eV) for (□) 100/0, (■) 99/1, (○) 95/5, (●) 90/10 and (Δ) 80/20 (wt/wt%) PVA/ $Cu(NO_3)_2.3H_2O$ composite films

show the PVA peaks but with small shifts and different intensities. The shift and the change in peaks intensity are clear signs of the formation of charge transfer complex between $Cu(NO_3)_2.3H_2O$ and PVA molecules. However, the peak position of the bands at 3369 cm^{-1} and 3276 cm^{-1} up to 5 wt% $Cu(NO_3)_2.3H_2O$ is significantly shifted, whereas these bands overlapped beyond this concentration. This may be due to the physical interaction between PVA and $Cu(NO_3)_2.3H_2O$.

Optical studies

The UV-Vis absorption spectra of pure PVA and PVA/ $Cu(NO_3)_2.3H_2O$ composite films are shown in Fig. 3. The absorbance spectrum of pure PVA reveals a shoulder like peak at 280 nm, which was due to the π-π* transition from unsaturated bonds, mainly (C=O and/or C=C) in the polymer [4, 21]. In general the absorbance of composite films increases

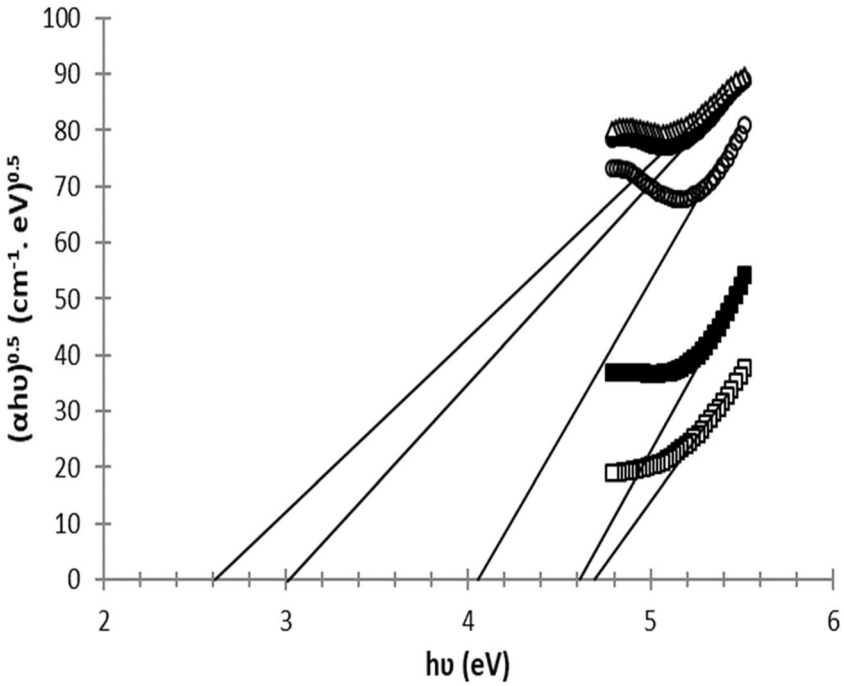

Fig. 6 Relation between $(\alpha h)^{0.5}$ $(cm^{-1}. eV)^{0.5}$ versus hυ (eV) for (□) 100/0, (■) 99/1, (○) 95/5, (●) 90/10 and (Δ) 80/20 (wt/wt%) PVA/ $Cu(NO_3)_2.3H_2O$ composite films

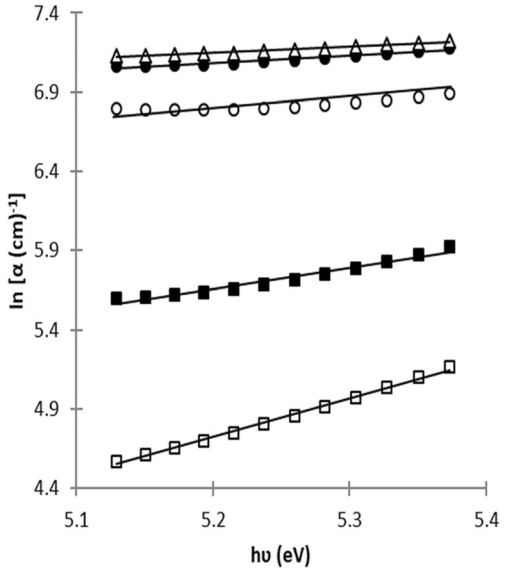

Fig. 7 Relation between ln [α (cm^{-1})] versus hυ (eV) for (□) 100/0, (■) 99/1, (○) 95/5, (●) 90/10 and (Δ) 80/20 (wt/wt%) PVA/ $Cu(NO_3)_2.3H_2O$ composite films

with an increase in $Cu(NO_3)_2.3H_2O$ ratio. For all composite films, a new peak appears at approximately 255 nm with different intensity. This observation confirms the interaction between the filler and PVA matrix. The absorption coefficient α(λ) is calculated using the Beer Lambert's formula [22].

$$\alpha(\lambda) = 2.303\ \frac{A}{d} \tag{1}$$

Where d is the thickness of the film and A is the absorbance. Figure 4 illustrates the absorption coefficient α(λ) of pure PVA and PVA/ $Cu(NO_3)_2.3H_2O$ composite films versus hυ (eV). From the plot, the absorption edge; which is the value of the photon energy at zero absorption; is acquired by extrapolation of the linear relationship to zero absorption. The values obtained are given in Table 1. As the ratio of $Cu(NO_3)_2.3H_2O$ increases, the absorption edge values for the investigated samples decrease. This decrease can be ascribed to changes in PVA crystallinity induced by $Cu(NO_3)_2.3H_2O$ which are compatible with X-ray data. This may also reflect changes in the number of final states available according to the compositional ratio. The energy band gap E_g of the composite films was calculated using the Tauc relation [23].

$$\alpha h\upsilon = \beta\ (h\upsilon - Eg)^m \tag{2}$$

Where h is the incident photon energy, β is a constant and m is the power coefficient with the value that is determined by the type of possible electronic transitions. m = 1/2 or 2 for direct and indirect allowed transitions respectively. As illustrated in Figs. 5 and 6, the interception of extrapolations of the liner portions of $(\alpha h)^2$ and $(\alpha h)^{1/2}$ to zero absorption on h axis gives the values of direct and indirect optical band gap energy. For all investigated samples, the obtained values of direct and indirect optical band gap energy are shown in Table 1. Table 1 shows that the direct and indirect optical band gap values of PVA decreased as the content of $Cu(NO_3)_2.3H_2O$ increased. Due to the incorporation of copper nitrate as impurity in the PVA matrix, the reduction of energy band gap is due to the formation of trap levels within the band gap. The increase in density of trap levels leads to narrowing of the band gap.

The absorption coefficient obeys Urbach empirical relation [24].

$$\alpha(\upsilon) = \alpha_0 \exp\left(\frac{h\upsilon}{E_U}\right) \tag{3}$$

Where α_0 is a constant and E_U (Urbach energy) is the width of the tail of the localized states within the band gap. The values of E_U were calculated from reciprocal of slopes of the linear portions of the graphs shown in Fig. 7 and given in Table 1. The E_U values increase with an increase in $Cu(NO_3)_2.3H_2O$ ratio in the composite system indicating a rise in number of charge trapping centers.

Electrical studies

Dielectric modulus

The frequency dependence of dielectric modulus allows one to obtain information on the relaxation processes in the studied samples [25–28]. The advantage of this impersonation is the minimization of the effects of electrode polarization. The complex dielectric modulus (M^*) is calculated using the following equation [25–28]

$$M^*(\omega) = \frac{1}{\varepsilon^*(\omega)} = M'(\omega) + i\,M'' = \frac{\varepsilon'}{\varepsilon'^2 + \varepsilon''^2} + i\,\frac{\varepsilon''}{\varepsilon'^2 + \varepsilon''^2} \tag{4}$$

where M' and M" are real and imaginary parts of dielectric modulus. Figure 8 demonstrates the dependence of the real part of the dielectric modulus M' on frequency at various temperatures for all studied samples. It is noted that at low frequency the M' approaches to zero due to the electrode polarization effect is dominant and increases with frequency and reaches the maximum value at high frequency. The s-shaped graph shows the ionic nature of the materials [29]. Fig. 9 shows the frequency dependence of M" at different temperatures for all studied samples. In all samples, a bell-shaped peak was noted. This peak is evident of relaxation transition. The bell shaped peaks are found to move to higher

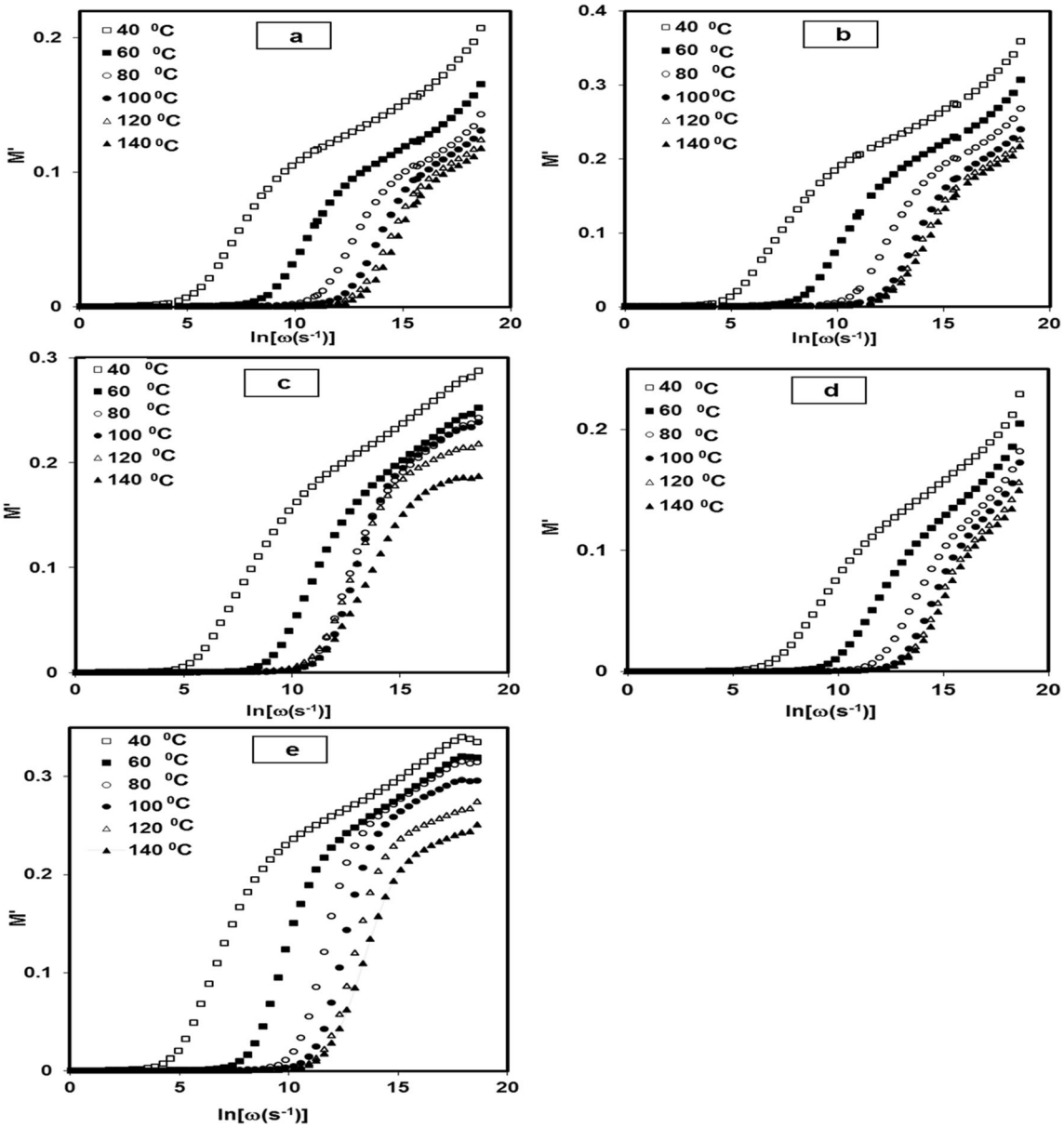

Fig. 8 The relation between the frequency and M' of **a** 100/0, **b** 99/1, **c** 95/5, **d** 90/10 and **e** 80/20 (wt/wt%) PVA/ $Cu(NO_3)_2.3H_2O$ composite films at different temperatures

frequencies with raising temperature in all examined samples. The frequency region below the peak maximum determines the range in which charge carriers occur due to long range hopping. The carriers are restricted to potential wells at frequencies above the peak maximum and therefore, are mobile for only short distances [30–33]. This type of behavior indicates the presence of a temperature dependent hopping mechanism for electrical conduction. The frequency (ω_m) at which the maximum, M''_{max}, is found defines the relaxation time (τ_m) by $\omega_m \tau_m = 1$. Table 2 represents the conductivity relaxation time (τ_m) for all composite samples at different temperatures. For all composite samples, the relaxation time decreases as temperature increases. A plot of ln (τ_m) as function of reciprocal temperature for all composites are shown in Fig. 10. The points show the experimental data, while the solid lines show the least square fit according to Arrhenius Equation [34],

$$\tau_m = \tau_0 e^{(\Delta E/kT)} \quad (5)$$

Where τ_o is the high temperature limit of the relaxation time, k is Boltzmann's constant, T is the absolute temperature and ΔE is the activation energy for conductivity relaxation. Figure 10 shows the existence of two slopes for all samples

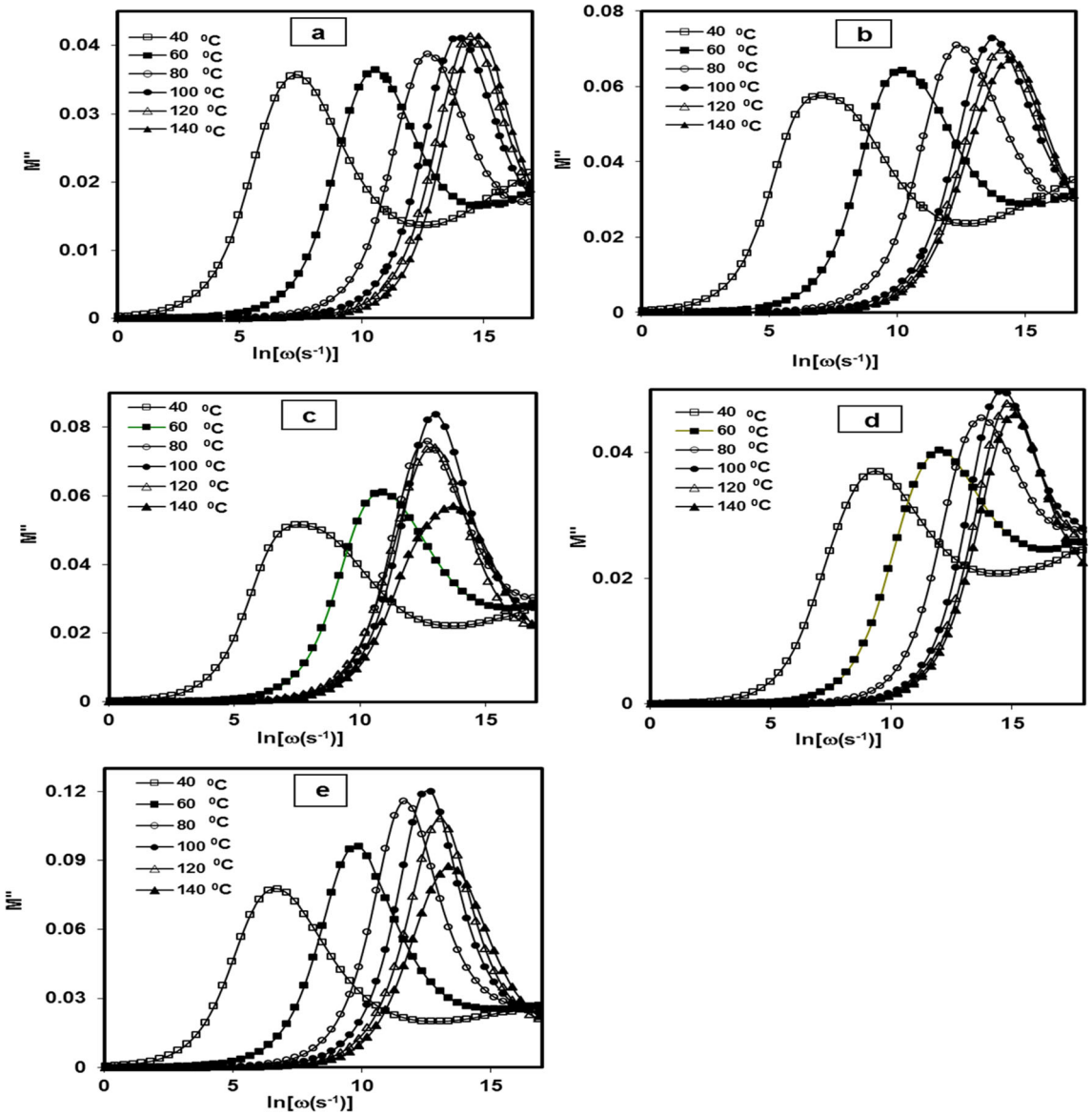

Fig. 9 The relation between the frequency and M" of **a** 100/0, **b** 99/1, **c** 95/5, **d** 90/10 and **e** 80/20 (wt/wt%) PVA/ $Cu(NO_3)_2.3H_2O$ composite films at different temperatures

that indicate the existence of two activation energies. The values of the activation energy for the composite samples have been calculated from the Arrhenius fit corresponding to Eq. 5; the values were shown in Table 3.

Table 2 Conductivity relaxation time of PVA/ $Cu(NO_3)_2.3H_2O$ composite films

Film composition PVA/ $Cu(NO_3)_2.3H_2O$ (wt/wt%)	Conductivity relaxation time, τ (sec.)					
	40 °C	60 °C	80 °C	100 °C	120 °C	140 °C
100/0	6.75×10^{-4}	2.75×10^{-5}	2.76×10^{-6}	1.01×10^{-6}	5.04×10^{-7}	3.74×10^{-7}
99/1	9.12×10^{-4}	4.11×10^{-5}	4.12×10^{-6}	1.02×10^{-6}	5.57×10^{-7}	4.56×10^{-7}
95/5	5.00×10^{-4}	2.04×10^{-5}	3.37×10^{-6}	2.26×10^{-6}	2.26×10^{-6}	1.12×10^{-6}
90/10	9.14×10^{-5}	6.14×10^{-6}	1.01×10^{-6}	4.56×10^{-7}	3.38×10^{-7}	2.77×10^{-7}
80/20	13.6×10^{-4}	5.55×10^{-5}	8.29×10^{-6}	3.37×10^{-6}	2.26×10^{-6}	1.52×10^{-6}

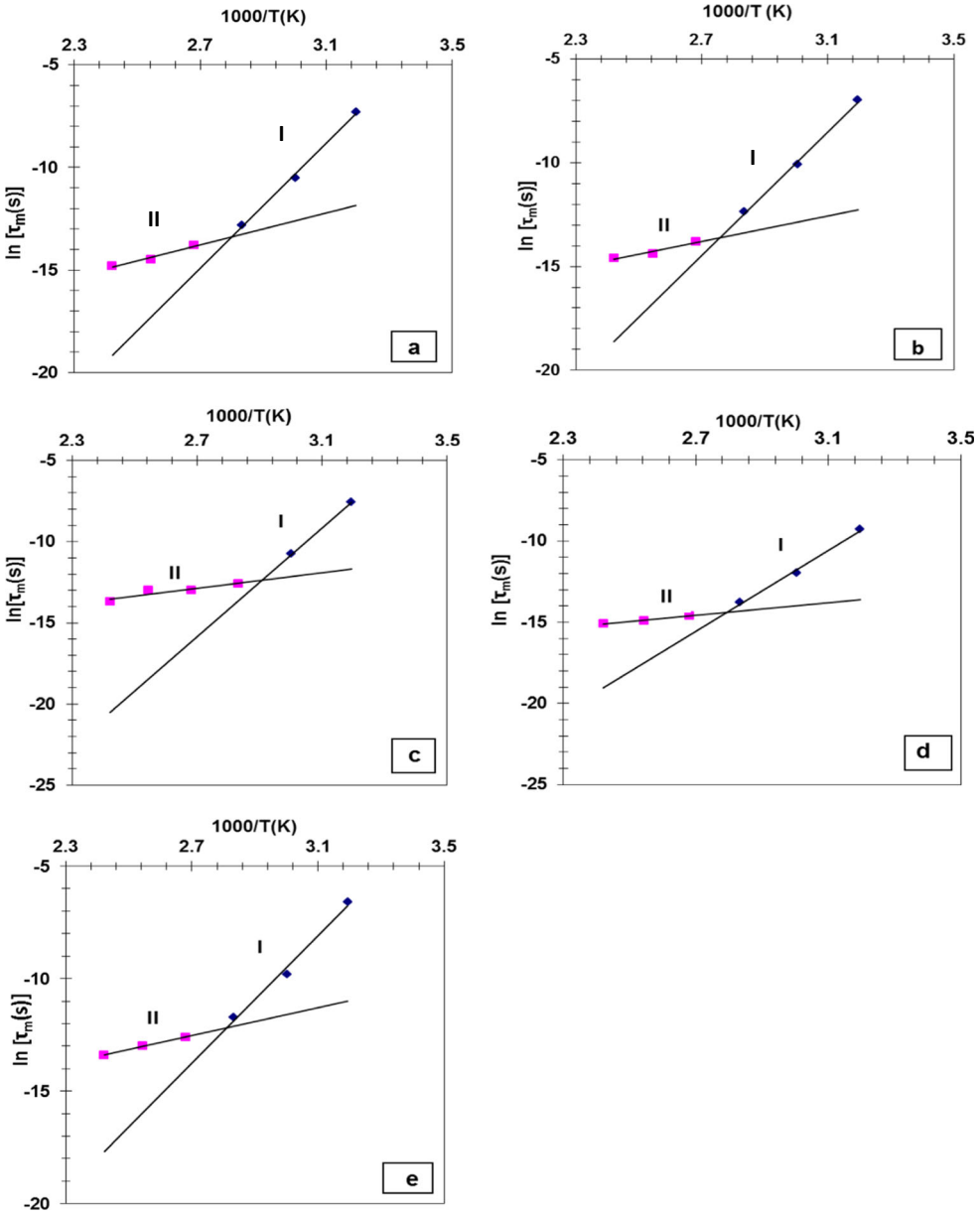

Fig. 10 The variation of ln [τ_m(s)] versus 1000/T(K) for: **a** 100/0, **b** 99/1, **c** 95/5, **d** 90/10 and **e** 80/20 (wt/wt%) PVA/ $Cu(NO_3)_2.3H_2O$ composite films. The solid line displays the fitting according to Eq. (5)

Electrical conductivity

The dependence of real part of electrical conductivity ln(σ) on reciprocal temperature at a selected frequency 1 kHz for pure PVA and PVA/ $Cu(NO_3)_2.3H_2O$ composite films is shown in Fig. 11. The conductivity increases with increasing temperature in a manner following Arrhenius type relation.

$$\sigma = A_0 e^{-\Delta E/kT} \quad (6)$$

Table 3 Activation energies of the conductivity relaxation for PVA/$Cu(NO_3)_2.3H_2O$ composite films according to Eq. (5)

Film composition PVA/ $Cu(NO_3)_2.3H_2O$ (wt/wt%)	ΔE_1 (eV)	ΔE_2 (eV)
100/0	1.31	0.33
99/1	1.28	0.27
95/5	1.43	0.21
90/10	1.07	0.16
80/20	1.22	0.26

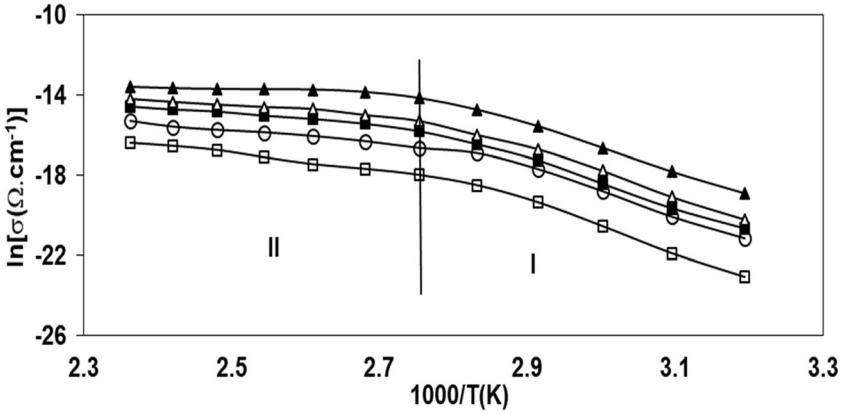

Fig. 11 The variation of ln $[\sigma(\Omega.cm)^{-1}]$ versus 1000/T(K) for: (□) 100/0, (■) 99/1, (Δ) 95/5, (▲) 90/10 and (o) 80/20 (wt/wt%) PVA/ $Cu(NO_3)_2.3H_2O$ composite films at 1 kHz

where ΔE is the activation energy, A_0 is the pre-exponential factor, k is Boltzmann constant and T is the temperature. For all samples, two distinct regions are identified as region I (313 < T < 353 K) and region II (T > 363 K).

Generally, the initial increase in conductivity with increasing temperature may be due the release of more charge carriers from traps and/or to greater mobility through the amorphous region of PVA matrix. Figure 11 demonstrates that the conductivity of composite samples is higher than that of pure PVA. At concentrations of 1, 5 and 10 wt% $Cu(NO_3)_2.3H_2O$ composite samples, the conductivity increases monotonically with an increase in doping ratio over the temperature range from 313 K – 415 K. This may be explained as a result of highly facilitated complex formation and the delocalization of more charge carriers transfer. It should be noted that the dopant concentration 10 wt% $Cu(NO_3)_2.3H_2O$ shows a maximum conductivity. On the other side, at concentration 20 wt% $Cu(NO_3)_2.3H_2O$ the conductivity decreases, and it remains higher than pure PVA. This can be attributed to the reduction in the mobility of charge carriers, mostly due to scattering of ionized molecular aggregates.

The activation energy ΔE for the different regions were calculated according to Eq. (6) and listed in Table 4. The values of ΔE suggest that the ion hopping mechanism may be assumed to be efficient in region I while the electron hopping mechanism in region II is effective. The lower values of activation energy are associated with the intermolecular conducting processes. While the higher values of activation energy are associated with the intramolecular conducting process. The intermolecular conducting process is less effective than the intramolecular one, because more charge carrier scattering is expected through the intermolecular covalent bonds than in the physical intramolecular bonds [35].

In general, the total conductivity can be represented by an empirical relation (universal power law) [36].

$$\sigma(\omega) = \sigma_{dc} + A\omega^{s} \quad (7)$$

where σ_{dc} is the dc conductivity, the factor A and the universal exponent s are both function of temperature and the conduction mechanism. Figure 12 displays the variation of the ac conductivity ln $[\sigma_{ac}(\omega)]$ versus frequency at chosen temperatures for pure PVA and PVA/ $Cu(NO_3)_2.3H_2O$ composite films. By linear fitting of σ_{ac} curves in Fig. 12, the values of exponent s were determined. Figure 13 illustrates the temperature variation of the exponent s for pure material and its composites. As observed from Fig. 13, with increasing temperature, the exponent s decreases and its value is less than unity i.e. 0 < s < 1. These findings therefore lead to the prediction that the correlated barrier hopping (CBH) is the most appropriate mechanism to describe the ac conduction behavior in the studied samples [37].

Table 4 Activation energy values for PVA/ $Cu(NO_3)_2.3H_2O$ composite films at 1 kHz according to Eq. (6)

Film composition PVA/ $Cu(NO_3)_2.3H_2O$ (wt/wt%)	ΔE_1 (eV)	ΔE_2 (eV)
100/0	1.113	0.371
99/1	1.032	0.232
95/5	1.027	0.201
90/10	1.005	0.056
80/20	1.034	0.253

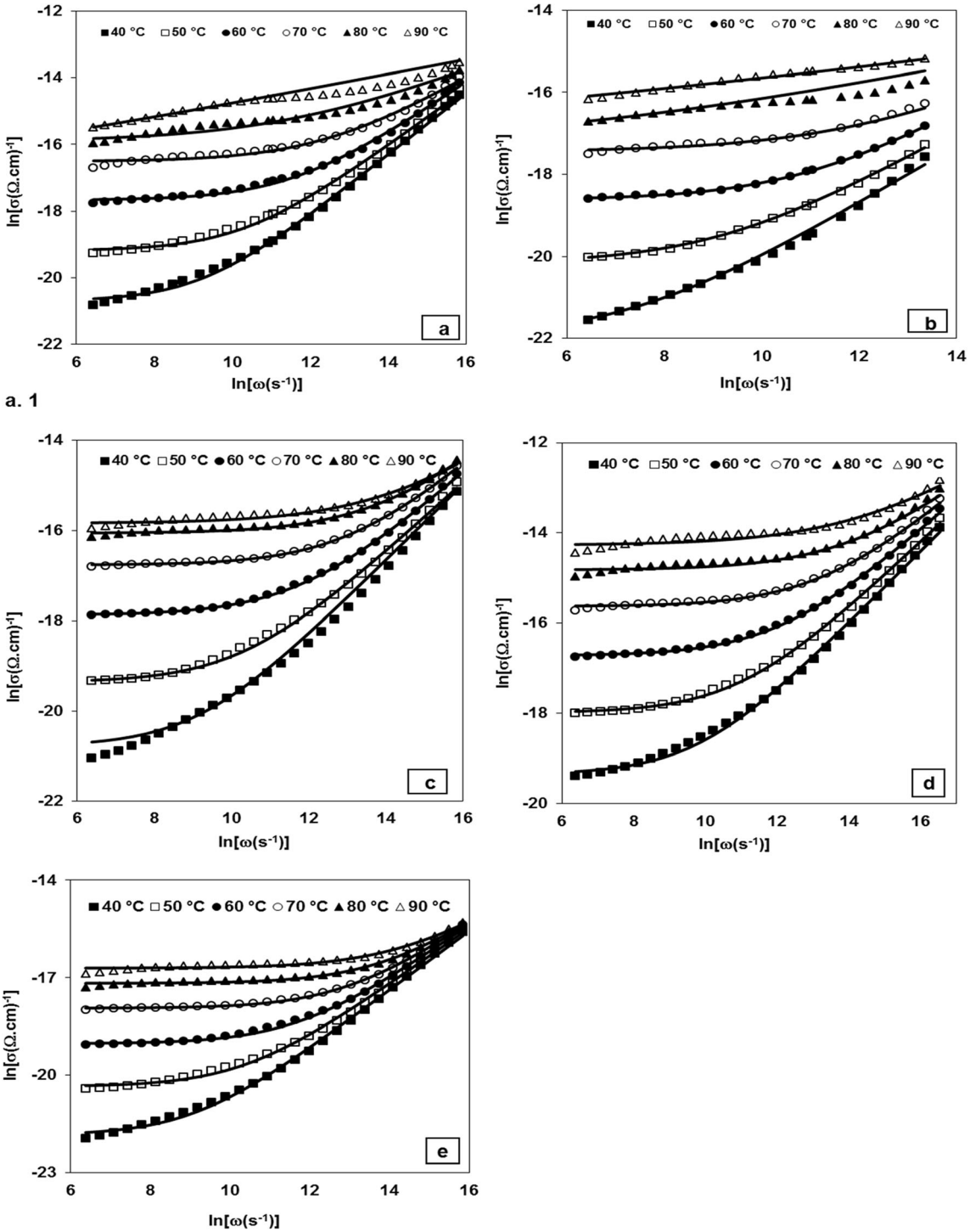

Fig. 12 Dependence of a.c. conductivity on frequency for: **a** 100/0, **b** 99/1, **c** 95/5, **d** 90/10 and **e** 80/20 (wt/wt%) PVA/ $Cu(NO_3)_2.3H_2O$ composite films. The solid lines display the fitting according to Eq. (7)

Conclusions

The inorganic salt $Cu(NO_3)_2.3H_2O$ was used in this paper to doped into PVA by casting method to improve its physical properties. The prepared samples were subjected to study the structural, optical and electrical properties. The chemical interaction between $Cu(NO_3)_2.3H_2O$ and PVA chain in composite films has been identified using XRD and FT-IR techniques.

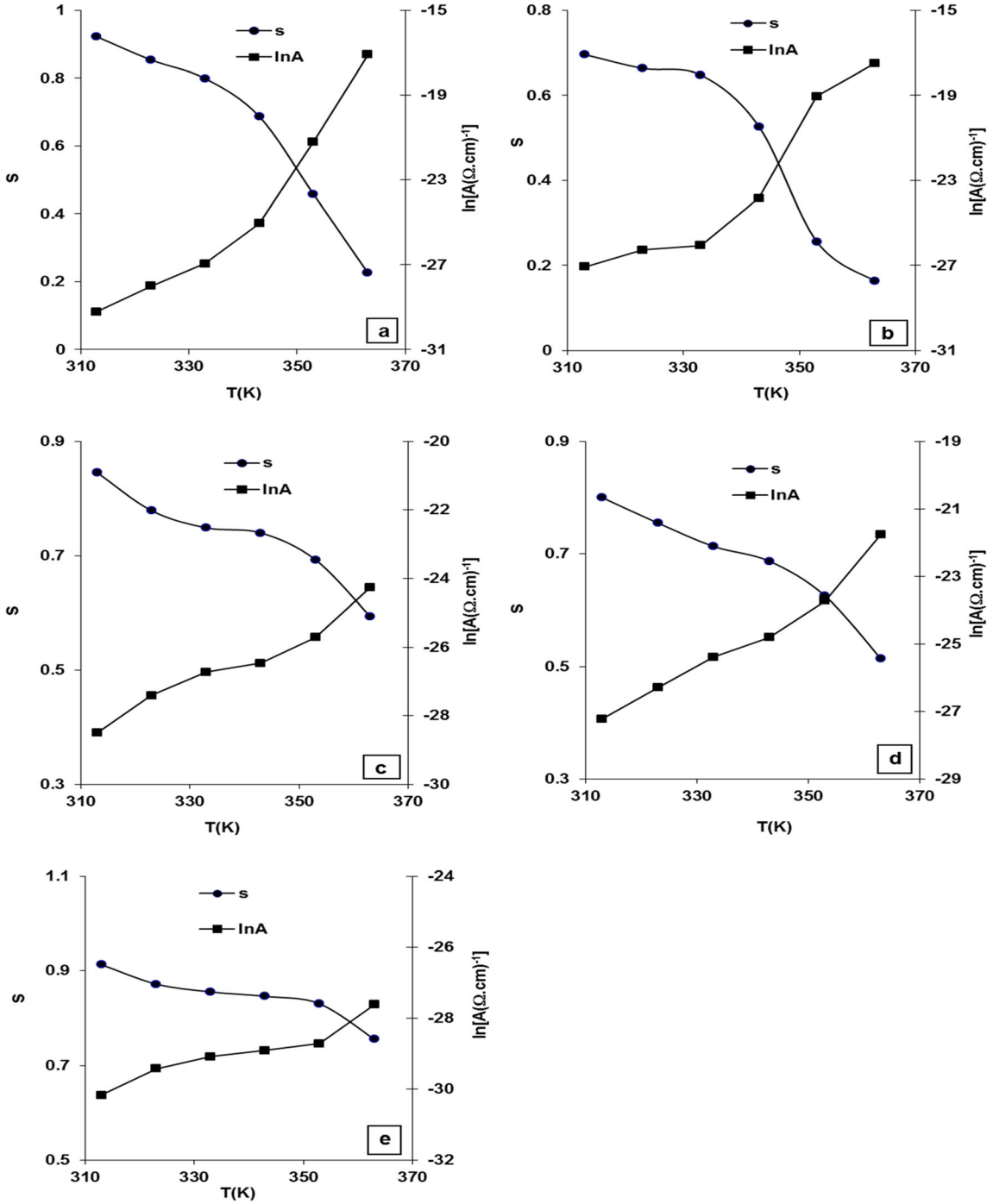

Fig. 13 Thermal variation of the factor A and exponent s for: **a** 100/0, **b** 99/1, **c** 95/5, **d** 90/10 and **e** 80/20 (wt/wt%) PVA/ $Cu(NO_3)_2.3H_2O$ composite films. The solid lines display the fitting according to Eq. (7)

$Cu(NO_3)_2.3H_2O$ could interact with PVA chain via hydrogen bonding between the ions and the hydroxyl group. Adding $Cu(NO_3)_2.3H_2O$ reduces the degree of crystallinity of PVA. The red shift for the absorption edge of the composite samples and the reduction in the optical energy gap, which is caused due to the change in the crystallinity within PVA matrix, confirmed the complexation between $Cu(NO_3)_2.3H_2O$ and PVA. The dielectric modulus plots indicate the single phase character of the composite samples. The electrical conductivity increased with increasing $Cu(NO_3)_2.3H_2O$ content in the host material up to 10 wt% because the increase of the effective free volume in the polymer matrix. On further increase of

ratio of inorganic salt, the electrical conductivity values decreased, indicating the inhomogeneous distribution of $Cu(NO_3)_2.3H_2O$. The correlated barrier hopping (CBH) is the dominant mechanism that describe the ac conduction behavior in the studied composite samples.

References

1. Kimura T, Kajiwara M (1998) Electrical properties of poly(n-butylamino) (di-allylamino)phosphazene. J Mater Sci 33:2955–2959
2. Yamaura K, Naitoh M (2002) Preparation of high performance films from poly(vinyl alcohol)/NaCl/H_2O systems. J Mater Sci 37:705–708
3. Zidan HM (2003) Structural properties of CrF_3- and $MnCl_2$-filled poly(vinyl alcohol) films. J Appl Polym Sci 88:516–521
4. Bhajantri RF, Ravindrachary V, Harisha A, Crasta V, Nayak SP, Poojary B (2006) Microstructural studies on $BaCl_2$ doped poly(vinyl alcohol). Polymer 47:3591–3598
5. Zidan HM (1999) Effect of $AgNO_3$ filling and UV-irradiation on the structure and morphology of VA films. Polym Test 18:449–461
6. Zidan HM (2003) Filling-level effect on the physical properties of $MgBr_2$- and $MgCl_2$- filled poly(vinyl acetate) films. J Polym Sci B Polym Phys 41:112–119
7. Abdelaziz M (2004) Effect of CsBr-$MnCl_2$ mixed fillers on the crystal structure and optical and electrical properties of poly(vinyl alcohol). J Appl Polym Sci 94:2178–2186
8. Kumar HGN, Rao JL, Gopal NO, Narasimhulu KV, Chakradhar RPS, Rajulu AV (2004) Spectroscopic investigations of Mn^{2+} ions doped polyvinyl alcohol films. Polymer 45:5407–5415
9. Kubo JI, Rahman N, Takahashi N, Kawai T, Matsuba G, Nishida K, Kanaya T, Yamamoto M (2009) Improvement of poly(vinyl alcohol) properties by the addition of magnesium nitrate. J Appl Polym Sci 112:1647–1652
10. Jiang XC, Zhang XF, Ye DZ, Zhang X, Dai H (2012) Modification of poly(vinyl alcohol) films by the addition of magnesium chloride hexahydrate. Polym Eng Sci 52:1565–1570
11. Jiang XC, Jiang T, Zhang XF, Zhang X, Dai H (2013) The plasticizing effect of calcium nitrate on poly(vinyl alcohol). Polym Eng Sci 53:1181–1186
12. Jiang XC, Jiang T, Zhang XF, Zhang X, Dai H (2012) Melt processing of poly(vinyl alcohol) through adding magnesium chloride hexahydrate and ethylene glycol as a complex plasticizer. Polym Eng Sci 52:2245–2252
13. El-Shahawy MA (2003) Phase transformations of some poly(vinyl alcohol)-$NiCl_2$ composites. Polym Int 52:1919–1924
14. Soliman Selim M, Seoudi R, Shabaka AA (2005) Polymer based films embedded with high content of ZnSe nanoparticles. Mater Lett 59:2650–2654
15. Wang DH (1996) Polyvinylalcohol film doped with CuCl nanoclusters. Thin Solid Films 288:254–255
16. Yu Y-H, Lin C-Y, Yeh J-M, Lin W-H (2003) Preparation and properties of poly(vinyl alcohol)- clay nanocomposite materials. Polymer 44:3553–3560
17. Rao JK, Raizada A, Ganguly D, Mankad MM, Satyanarayana SV, Madhu GM (2015) Enhanced mechanical properties of polyvinyl alcohol composite films containing copper oxide nanoparticles as filler. Polym Bull 72:2033–2047
18. Sonmez M, Ficai D, Stan A, Bleotu C, Matei L, Ficae A, Andronescu E (2012) Synthesis and characterization of hybrid PVA/Al_2O_3 thin film. Mater Lett 74:132–136
19. Rajendran S, Sivakumar M, Subadevi R (2004) Investigations on the effect of various plasticizers in PVA–PMMA solid polymer blend electrolytes. Mater Lett 58:641–649
20. Linga Raju CH, Rao JL, Reddy BCV, Brahmam V (2007) Thermal and IR studies of copper doped polyvinyl alcohol. Bull Mater Sci 30:215–218
21. Praveena SD, Ravindrachary V, Bhajantri RF, Ismayil (2016) Dopant-induced microstructural, optical, and electrical properties of TiO_2/PVA composite. Polym Compos 37:987–997
22. Abdullah GO, Saleem SA (2016) Effect of copper sulfide nanoparticles on the optical and electrical behavior of poly(vinyl alcohol) films. J Electron Mater 45:5910–5920
23. Mott NF, Davis NF (1979) Electronic process in non-crystalline materials.2nd edn. Oxford University Press, Oxford
24. Urbach F (1953) The long-wavelength edge of photographic sensitivity and of the electronic absorption of solids. Phys Rev 92:1324
25. Tsangaris GM, Psarras GC, Kouloumbi N (1998) Electric modulus and interfacial polarization in composite polymeric system. J Mater Sci 33:2027–2037
26. Dokme I, Alundal S, Gokcen M (2008) Frequency and gate voltage effect on the dielectric properties of Au/SiO_2/n-Si structure. Microelectron Eng 85:1910–1914
27. Tekeli Z, Gokcen M, Alundal S, Ozcelik S, Ozbay E (2011) On the profile of frequency dependent dielectric properties of (Ni/Au)/GaN/$Al_{0.3}Ga_{0.7}N$ heterostructure. Microelectron Reliab 51:581–586
28. Pakma O, Serin N, Serin T, Alundal S (2008) Influence of frequency and bias voltage on dielectric properties and electrical conductivity of Al/TiO_2/p-Si/p^+ (MOS) structures. J Phys D Appl Phys 41:215103
29. Macedo PB, Moynihan CT, Bose R (1972) The role of ionic diffusion in polarisation in vitreous ionic conductors. Phys Chem Glasses 13:171
30. Mohamed Ali T, Padmanathan N, Selladurai S (2013) Structural, conductivity and dielectric characterization of PEO–PEG blend composite polymer electrolyte dispersed with TiO_2 nanoparticles. Ionics 19:1115–1123
31. Arya A, Sharma AL (2018) Structural, electrical properties and dielectric relaxations in Na^+-ion-conducting solid polymer electrolyte. J Phys Condens Matter 30:165402 (26 pp)
32. Arunkumar R, Babu RS, Usha Rani M (2017) Investigation on Al_2O_3 doped PVC–PBMA blend polymer electrolytes. J Mater Sci Mater Electron 28:3309–3316
33. Shobhna C (2018) Characterization of amorphous silica nanofiller effect on the structural, morphological, optical, thermal, dielectric and electrical properties of PVA-PVP blend based polymer nanocomposites for their flexible nanodielectric applications. J Mater Sci Mater Electron 29:10517–10534
34. Hanafy TA, Elbanna K, El-Sayed S, Hassen A (2011) Dielectric relaxation analysis of biopolymer poly(3-hydroxybutyrate). J Appl Polym Sci 121:3306–3313
35. Madani M, Maziad NA, Khafagy RM (2007) Thermally stimulated depolarization current and thermal analysis studies of gamma irradiated lithium-salt/polymer electrolyte blends. J Macromol Sci B Phys 46:1191–1203
36. Jonscher AK (1983) Dielectric relaxation in solids, P340. Chelsea Dielectric Press, London
37. Dulta M, Kunda RS, Hooda J, Murugavel S, Punia R, Kishore N (2015) Temperature and frequency dependent conductivity and electric modulus formulation of manganese modified bismuth silicate glasses. J Non-Cryst Solids 1:423–424